LUND UNIVERSITY

FACULTY OF SCIENCE

Dynamic and static axial symmetry breaking in nuclei

Lucas H. Jakander

Thesis submitted for the degree of Bachelor of Science
Project duration: 2 months, 15 ECTS

Supervisor: Gillis Carlsson
Co-supervisor: Andrea Idini

Department of Physics
Division of Mathematical Physics
June 2026

Contents

List of abbreviations

- HFB - Hartree-Fock-Bogoliubov
- GCM - Generator Coordinate Method
- PNP - Particle Number Projection
- AMP - Angular Momentum Projection
- RAMP - Restricted Angular Momentum Projection
- irrep - Irreducable representation
- CHFB - Constrained HFB
- PCHFB - Projected CHFB
- MPCHFB - Mixed PCHFB

Abstract

In the collective model of the atomic nucleus, oscillations in the quadrupole deformation naturally arise; a type of these dynamic shape fluctuations are known as γ-vibrations. However, features attributed to these vibrational modes may instead arise from static triaxiality through configuration mixing. This thesis explores a possible way to avoid this ambiguity. Whilst single phonon γ-vibrations are firmly established the search for pure double phonon $\gamma\gamma$-vibrations is currently underway. And thus, a good theoretical understanding of γ-vibrations would be beneficial. The central idea of this work is to suppress the rotational copies of the intrinsic shape by restricting the rotational degree of freedom to a single axis in the nuclear model. Two nuclei, ^{24}Mg and ^{32}S, were investigated and both showed behaviour characteristic of γ-vibrational modes. The results furthermore agree closely with the Bohr Hamiltonian thus affirming the interpretation of γ-vibrations as true dynamic shape fluctuations.

Populär vetenskaplig sammanfattning

Tänk dig att du har en elastisk boll (till exempel en sfärisk ballong), en som du kan dra och pressa ihop till ditt hjärtas begäran. De former, eller deformationer, du kan skapa genom att dra och pressa kallas, med den tjusiga termen, *kvadrupoldeformationer*. Genom att dra bollen längs en linje (en *axel*) får du en *prolat* form vilket liknar en amerikansk fotboll, och om du istället pressar längs den axeln får du en pannkaka som kallas en *oblat* form. Med hjälp av en vän kan du dra och pressa längs två olika axlar och därmed få en form någonstans mellan den prolata och oblat formen som kallas triaxial.

Samma former, dessa kvadrupoldeformationer, kan beskriva formen på kärnan av en atom (*atomkärnan*). Atomkärnor är dock otroligt små (i storleksordningen av några femtometer det vill säga 10^{-15} meter), och styrs därför av kvantmekanikens lagar. Det är här vår beskrivning blir förvirrande och abstrakt. Du förstår, ett välkänt fenomen inom kvantmekaniken är det som kallas superposition: en partikel kan befinna sig på två platser samtidigt. I vårt fall innebär detta att en kärna kan anta två former samtidigt.

Med lite energi observerar vi fluktuationer i atomkärnans form, något vi sedan tolkar som *vibrationer*. Vi observerar detta som en blandning av flera former som beskriver vår kärna. När de blandade formerna är triaxiella kallar vi detta en γ-vibration (gamma-vibration).

Problemet är att det finns en viss tvetydighet om huruvida blandningen av former faktiskt beror på en dynamisk fluktuation: då man kan få samma bild med en statiskt deformerad atomkärna genom att endast rotera den i rymden.

Med hjälp av datorer kan vi skapa ett modellsystem som beskriver kärnor från grunden genom att använda kvantmekaniska principer. Vi kan sedan styra symmetrin i vårt modellerade system med hjälp av en *projektionsoperator*, vilket kan betraktas som ett filter, som tar bort alla oönskade delar. Vi skapade en sådan projektionsoperator för att begränsa rotationssymmetrin till en axel. Tanken är att om vi tar bort möjligheten för atomkärnan att rotera och vi fortfarande observerar en γ-vibration, så kan vi med säkerhet säga att detta är en dynamisk formfluktuation.

Två kärnor studerades, ^{24}Mg (magnesium) och ^{32}S (svavel). Först visade en analys av den begränsande modellen att den fungerade som förväntat och gav en snabbare beskrivning av naturen än dess obegränsande motsvarighet. Det viktiga är att den begränsande modellen ger en korrekt beskrivning av en atomkärna som är rotationsfixerad i rymden. Det upptäcktes sedan att γ-vibrationerna kvarstod i den begränsande modellen för båda dessa kärnor. Detta bekräftar tolkningen av γ-vibrationer som sanna vibrationstillstånd.

Popular science summary

Imagine you have an elastic ball (a spherical balloon for example), one you can pull and squish to your heart's desire. The shapes, or deformations, you can produce by you pulling and squishing are called by the fancy term *quadrupole deformations*. Pulling the ball along one line (an *axis*) you obtain a *prolate* shape similar to an American football, and if you instead squeeze along that axis you get a pancake called an *oblate* shape. By the help of a friend you may pull and squeeze along two different axes and thus obtain a shape somewhere in between the prolate and oblate called *triaxial*.

The very same shapes, these quadrupole deformations, can describe the shape of the core of an atom (the *nucleus*). However, nuclei are incredibly small (on the order of femtometers that is 10^{-15} meters), and thus are governed by the the laws of *quantum mechanics*. It is here where our description becomes confusing and abstract. See, a common phenomenon of quantum mechanics is what is called *superposition*: a particle can be at two places at once. In our case, this translates to the fact that a nucleus can obtain two shapes at once.

With a little bit of energy we observe fluctuations in the nucleus' shape, something we then interpret as *vibrations*. We observe this as the *mixing* of several shapes adhering to our nucleus. When the mixed shapes are triaxial we call this a γ-vibration (gamma-vibration).

The issue is that there exists some ambiguity to whether the mixing of shapes is in fact due to a dynamic fluctuation: one could obtain the same picture with a statically deformed shape by simply rotating it in space.

By the use of computers we may create a model system describing nuclei from the ground up by using the quantum mechanical principles. We can then control the symmetry of our modeled system by the use of a *projection operator*, which can be thought of as a filter, removing all undesirable parts. We created one such projection operator to restrict the rotational symmetry to one axis. The idea is that if we remove the possibility for the nucleus to rotate and we still observe a γ-vibration then we can say for sure that this is a dynamic shape fluctuation.

Two nuclei were studied, ^{24}Mg (magnesium) and ^{32}S (sulfur). First an analysis of the restricted model revealed that it functioned as expected yielding a faster description of nature than its unrestricted counterpart. The important note is that the restricted model produces a correct description of a nucleus rotationally fixed in space. It was then found that the γ-vibrations persisted in the restricted model for both of these nuclei. Thus affirming the interpretation of γ-vibrations as true vibrational states.

Acknowledgments

I thank my supervisors, Gillis Carlsson and Andrea Idini, for explaining and guiding me through this project. You made the several thousands of lines of Fortran code seem much less insurmountable. Tack Maite, min kära sambo, för det lugn och den trygghet du har gett mig. And finally, I thank my office mates, Kyra and Lasse, for making the stressful periods manageable and maybe even fun. Sorry for knocking on the door even though I had the card ready.

I acknowledge the use of generative artificial intelligence for code debugging, plotting and minor paraphrasing.

1 Introduction

In analogy to a particle in a harmonic oscillator potential, the atomic nucleus' shape should include vibrational modes at higher excitations. However, even with a perfect nuclear wavefunction in hand, the characterisation of excited states remain a challenge. The issue lies with total angular momentum conservation blurring the picture. Because of this the identification of a nuclear state as a superposition of two deformed shapes can be explained either as two copies of the same statically deformed state only rotated in space, or as a nucleus in a vibrational excitation dynamically transitioning between the two nuclei.

It was with the introduction of the collective model by Bohr and Mottelson [1, 2] that the collective variables β and γ were introduced to describe nuclear deformations. These parameters can be defined after considering the macroscopic liquid drop model [3]. In this semi-classical model (and also collective nuclear models), the deformed nuclear surface is parametrized by expanding the radial distance $R(\theta, \phi)$ from the center of mass in terms of spherical harmonics $Y_{\lambda\mu}(\theta, \phi)$. To do this for quadrupole deformations, we set $\lambda = 2$ and thus we obtain five parameters, $a_{2\mu}$ ($|\mu| \leq 2$), each acting as an expansion coefficient to its spherical harmonic $Y_{2\mu}(\theta, \phi)$. Although, these five can be reduced, as three need only determine the orientation in space. They correspond to the Euler angles and can thus be replaced by them. Thus, by the use of a suitable rotation, the five parameters reduce to only 2 real valued independent intrinsic shape variables a_{20} and $a_{22} = a_{2-2}$ relative to an axis plus the three Euler angles (note that $a_{21} = a_{2-1} = 0$). The coordinates of the intrinsic deformation plane, shown in Figure 1, are further defined as

$$a_{20} = \beta \cos(\gamma), \qquad a_{22} = \frac{1}{\sqrt{2}} \beta \sin(\gamma). \tag{1}$$

The radial function describing the intrinsic shape takes the form,

$$R(\theta, \phi) = R_0 \left(1 + \beta \sqrt{\frac{5}{16\pi}} \left(\cos\gamma (3\cos^2\theta - 1) + \sqrt{3} \sin\gamma \sin^2\theta \cos 2\phi \right) \right). \tag{2}$$

From here it is noticeable that β describes the departure from sphericity whilst γ describe the departure from axial symmetry, something which is further visualised in Figure 1.

By the use of these parameters one can describe all quadrupole deformations as points on a plane. At the origin ($\beta = 0$) one has the spherical shape, being rotationally symmetric about all axes. Prolate shapes, ($\beta > 0, \gamma = 0^\circ, 120^\circ$ or -120°), and oblate shapes, ($\beta > 0, \gamma = 180^\circ, -60^\circ$ or 60°), are axially symmetric: meaning that they are rotationally symmetric about one axis (z, x or y exclusively). The remaining shapes existing in the deformation

plane are triaxial, being rotationally symmetric about no axis and thus corresponding to axial symmetry breaking. Since most of the deformation plane is redundant one often restricts the plane to the first sextant restricting the domains as: $\beta \in [0, \infty]$ and $\gamma \in [0°, 60°]$.

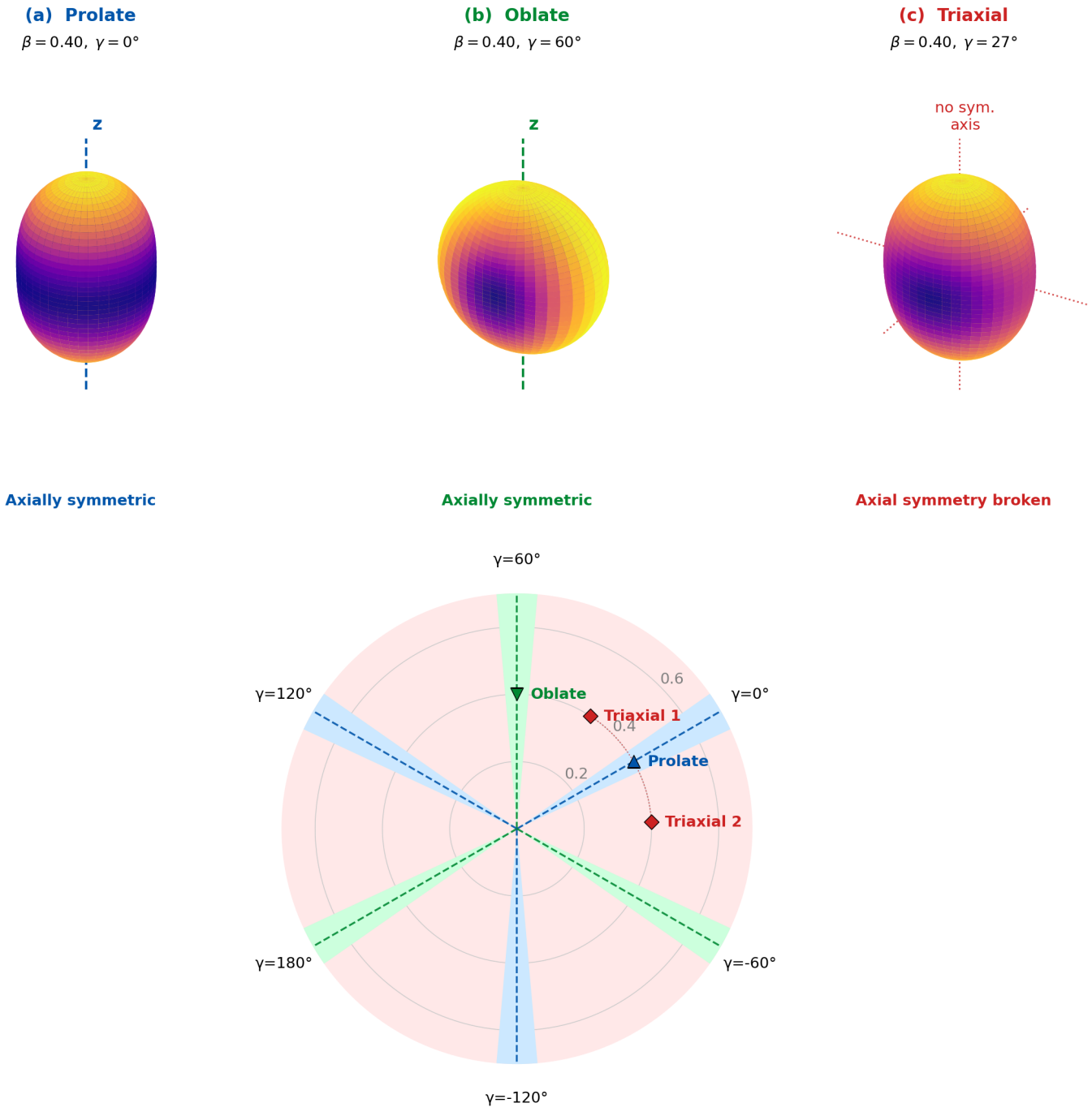

Figure 1: Illustration of nuclear shapes and their locations in the full deformation plane defined by the collective variables β the radial component describing the departure from sphericity and γ the angular component describing the departure from axial symmetry.

A γ-vibrational nucleus is conventionally understood as a nuclear system exhibiting dynamic axial-symmetry breaking, where the nuclear shape oscillates in the γ degree of freedom. In such a picture, the nucleus can be viewed as a superposition of two triaxial configurations, each located symmetrically with respect to the $\gamma = 0^\circ$ axis. These two configurations are related by rotation and therefore represent rotational counterparts of one another.

However, this interpretation relies critically on knowing the intrinsic shape of the nucleus and thus the identification of a γ band as vibrational excitations becomes ambiguous. Features attributed to γ-vibrations may instead arise from static triaxiality through configuration mixing. Thus, without a clearer understanding of the underlying shape's time evolution, one cannot confidently assert that a γ-vibrational nucleus truly represents a vibrational mode.

This thesis explores a possible way to avoid this ambiguity. The central idea is to suppress the rotational copies of the intrinsic shape by restricting the rotational degree of freedom to a single axis in the nuclear model. By eliminating the rotationally equivalent triaxial configurations, the model may provide a diagnostic tool for distinguishing dynamic from static axial symmetry breaking. At the same time, such a restriction inevitably reduces the model's accuracy, so an important part of this work is to investigate how the predicted nuclear spectra are affected and to what extent meaningful physical conclusions can still be drawn.

2 Background

The model used in this work utilises the mixing of mean field states along with the projection method for symmetry restoration. The following introduces the central concepts considered in this work.

2.1 γ-vibrations

Triaxial nuclei are expected to be seen all over nuclear chart [4] and the one-phonon γ-vibrational state is a well established interpretation of the the first excited band with $K^\pi = 2^+$ [2] for even-even nuclei. Currently experiments probing two-phonon γ-vibrations are underway with ^{164}Dy as a strong candidate [5].

From the Bohr Hamiltonian, the five-dimensional collective Hamiltonian describing quadrupole nuclear motion in terms of the shape variables β and γ together with the three Euler angles, incorporating both vibrational and rotational kinetic energies as well as a collective potential, it follows that the band head of the gamma vibrational state will lie at $\hbar\omega_\gamma$ above the ground state [3], this depends on the frequency of the γ-vibration,

$$\omega_\gamma = \sqrt{\frac{C_{22}}{B_2}}. \tag{3}$$

Here C_{22} is the stiffness of the γ oscillator potential and B_2 is the collective inertia coefficient. Using the relation $B_2 \propto A^{\frac{5}{3}}$ [3] one can derive the ratio of the γ-vibrational excitation energy for two nuclei, each with mass number A and A',

$$\frac{\omega_\gamma^A}{\omega_\gamma^{A'}} = \sqrt{\frac{C_{22}^A}{C_{22}^{A'}} \cdot \left(\frac{A'}{A}\right)^{5/3}}., \tag{4}$$

This is an approximation that assumes the nucleus to be a rigid body of a well defined shape and the two nuclei to have similar deformations.

2.2 Hartree-Fock-Bogoliubov method

In early attempts to describe the complicated quantum many body system that is the nucleus, it helped to make the assumption that nucleons move independently within a shared potential. This assumption was justified by the success of the nuclear shell model, for example by its ability to predict magic numbers and is the core idea behind mean-field theories which reduces the complicated N-body problems to a manageable one-body problem.

The Hartree-Fock-Bogoliubov (HFB) method is one such self-consistent mean-field model,

widely used with great effect to describe incorporating pairing along with the mean field effects of nuclei simultaneously. It builds upon the simpler Hartree-Fock (HF) method which describes the N-body wavefunction of a given nucleus as a single slater determinant,

$$|HF\rangle = \prod_{i=1}^{N} a_i^\dagger |0\rangle. \tag{5}$$

Here the particle creation operators $a_i^\dagger$ each correspond to a single particle state when acting on the vacuum state $|0\rangle$. The approximated true state is then found by the HF method through minimising the total energy of a system within the restricted space of this single Slater determinant. (A more detailed describtion may be found in Ref. [3] from page 189).

The HFB method then aims to incorporate pairing, the phenomenon where nucleons favour forming pairs coupled to the lowest total angular momentum, $I = 0$. This is done by introducing quasi-particles which are linear combinations of particles and holes. The quasi-particle creation operator,

$$\beta_k^\dagger = \sum_l U_{lk} a_l^\dagger + V_{lk} a_l, \tag{6}$$

is thus a linear combination of creation and annihilation operators, $a_l^\dagger$ and a_l, mixed using the complex matrices U and V.

A HFB state $|\phi\rangle$ is then defined to be a vacuum with respect to all quasiparticles: $\beta_k|\phi\rangle = 0$, $\forall\beta_k$ and thus may be written as,

$$|\phi\rangle = \prod_k \beta_k |0\rangle. \tag{7}$$

(a more detailed view is given in Ref. [6]).

Make note that from this definition one does not obtain an eigenstate of the particle number operator, $\hat{N}$. In fact, it is a superposition of states with different particle numbers $(N, N \pm 2, N \pm 4, ...)$. This is related to the topic of spontaneous symmetry breaking which will be covered in more detail in section 2.5

2.3 Generator Coordinate Method

The Generator Coordinate Method (GCM), first introduced in 1953 by Hill and Wheeler [7], is a microscopic approach in nuclear physics well suited for modelling large-amplitude collective phenomena such as fission, clustering, and vibrational motion. It is a beyond-mean-field method, meaning it goes beyond the single Slater determinant description of HF or HFB by proposing that the true nuclear many-body state is a correlated superposition of

many such mean-field states,

$$|\Psi\rangle = \sum_{\lambda} h_{\lambda} |\phi_{\lambda}\rangle, \tag{8}$$

where each $|\phi_{\lambda}\rangle$ is a mean-field state labelled by a set of generator coordinates λ parametrising the collective degrees of freedom of the nucleus, such as quadrupole deformation. Applying the variational principle to Equation (8) yields the Hill-Wheeler equation,

$$\sum_{\lambda} H_{\lambda'\lambda}\, h_{\lambda} = E \sum_{\lambda} O_{\lambda'\lambda}\, h_{\lambda}, \tag{9}$$

a generalised eigenvalue problem defined in terms of the Hamiltonian and overlap matrices,

$$H_{\lambda'\lambda} = \langle \phi_{\lambda'} | \hat{H} | \phi_{\lambda} \rangle, \qquad O_{\lambda'\lambda} = \langle \phi_{\lambda'} | \phi_{\lambda} \rangle. \tag{10}$$

Solving Equation (9) yields the energies E and weight coefficients h_{λ} of the correlated states $|\Psi\rangle$. As the basis states $|\phi_{\lambda}\rangle$ are generally symmetry-broken mean-field states, the GCM is often combined with symmetry restoration techniques, which is the central focus of this work and is discussed in detail in section 2.5.

2.4 Constraining fields

Cranking, first introduced by Inglis [8], is a method which allows for the study of high-spin states of excited nuclei. The mean-field solutions, the HFB basis states, are each an approximation of the ground state which implies for even-even nuclei (even number of both protons and neutrons) that the total spin $I = 0$. The method of cranking circumvents this by transforming the nuclear Hamiltonian as $\hat{H} \to \hat{H} - \omega \hat{I}_x$. Now, the mean-field solution will still provide an approximation of the ground state, however, it will be in a rotating frame of reference (rotating with frequency ω around the x-axis) and thus will have average angular momentum $I > 0$ hence we call the state cranked as we have added a angular momentum to the system.

2.5 Projection method

As stated above, the mixing of HFB states provides a computationally efficient way of probing a multitude of nuclear phenomena. However, another result of this method is the breaking of symmetries of the nuclear Hamiltonian. The two striking examples are the symmetries of particle number and angular momentum. Without these symmetries we loose their respective conserved quantities [9] and thus can not label our states with these properties as good

quantum numbers.

The projection method offers a way to restore the broken symmetries and thus obtain good quantum numbers. Whilst this method can handle both discrete and continuous symmetries, here only the continuous case is treated and thus we concern ourselves with Lie groups: in particular $U(1)$ and $SU(2)$. The unitary group of degree 1, $U(1)$, is the abelian group associated with global gauge rotations. The special unitary group, $SU(2)$, is the non-abelian group associated with rotations in Hilbert space.

The main idea is to obtain a projection operator which may extract components with the correct symmetry from a symmetry violating state. The projection operator will take the form,

$$\hat{P}^{\mu}_{kl} = \frac{d_\mu}{v_G} \int_G dv_G(g) D^{\mu\,*}_{kl} \hat{U}(g). \tag{11}$$

Here μ represents the irreducible representations (irreps) of the group G, d_μ is the dimension of said irrep, v_G is the volume of the group, $dv_G(g)$ is the invariant measure (Haar Measure) of the group, $D^{\mu\,*}_{kl}$ is the complex conjugated irreducible matrix representation and $\hat{U}(g)$ is the unitary representation operator. This general form is defined from group theory and will be given a short introduction in the next section although a more detailed and rigorous description of these elements may be found in Ref. [10] and [11]).

2.5.1 Group theoretical description

For a short description of the general projection operator (Equation (11)) we consider a compact Lie group G. The volume v_G of the group is defined as the integral over the groups domain of definition which is calculated as

$$v_G = \int_G dv_G(g), \tag{12}$$

where $dv_G(g)$ is the invariant measure for G, called the Haar measure. For each element $g \in G$ we consider the unitary operator $\hat{U}(g)$ acting on the Hilbert space $\mathcal{H}$. This means, since we can decompose the Hilbert space into a direct sum of orthogonal, invariant subspaces, each carrying an irrep of the group,

$$\mathcal{H} = \bigoplus_\lambda S^\lambda, \tag{13}$$

the action of $\hat{U}(g)$ on a state $|\Psi^\lambda\rangle \in S^\lambda$ is then also in the same subspace: if $\{\psi^{\lambda i}\}$ with $i \in \{1, 2, \ldots, d_\lambda\}$ make up an orthonormal basis then we have,

$$\hat{U}(g)|\Psi^\lambda\rangle = \sum_{i=1}^{d_\lambda} D^{\mu}_{kl}(g)|\psi^{\lambda i}\rangle. \tag{14}$$

This superposition has coefficients $D^{\mu}_{kl}(g) = \langle \psi^{\lambda k} | \hat{U}(g) | \psi^{\lambda l} \rangle$. The great orthogonality theorem [10],

$$\frac{d_\mu}{v_G} \int_G dv_G(g)\ D^{\mu\,*}_{kl} D^{\lambda}_{ij} = \delta_{\mu\lambda}\delta_{ki}\delta_{lj}, \tag{15}$$

then implies that the projection operator may be defined as given in Equation (11): when acting on a basis function the projection operator will either annihilate states corresponding to a different irrep ($\lambda \neq \mu$) or transform the basis states within the irrep μ:

$$\hat{P}^{\mu}_{kl} |\psi^{\lambda i}\rangle = \delta_{\mu\lambda}\delta_{li} |\psi^{\mu k}\rangle. \tag{16}$$

2.5.2 Restoration of particle number and angular momentum

With this description now established, we can introduce the particle number projection (PNP) operator, restoring the particle number symmetry [11],

$$\hat{P}^N = \frac{1}{\pi} \int_0^{\pi} d\theta\ e^{-i\theta(\hat{N}-N)}, \tag{17}$$

here $\hat{N} = \sum_i a_i^\dagger a_i$ is the number operator, θ is the gauge angle and N is the desired particle number. This operator when applied to an eigenstate of the number operator $|N'\rangle$ will return 0 if $N' \neq N$ and 1 if $N' = N$. Furthermore, the angular momentum projection (AMP) operator, restoring angular momentum is [11],

$$\hat{P}^I_{MK} = \frac{2I+1}{8\pi^2} \int_0^{2\pi} d\alpha \int_0^{\pi} d\beta\ \sin(\beta) \int_0^{2\pi} d\gamma\ D^{I*}_{MK}(\alpha,\beta,\gamma) \hat{R}(\alpha,\beta,\gamma). \tag{18}$$

Here the parameters (α, β, γ) are the Euler angles (not to be confused with the collective variables β and γ), $\hat{R}(\alpha,\beta,\gamma) = e^{-i\alpha\hat{I}_z} e^{-i\beta\hat{I}_y} e^{-i\gamma\hat{I}_z}$ is the rotation operator with $\hat{I}_i$ being the angular momentum operator along the ith axis, and $D^I_{MK}(\alpha,\beta,\gamma) \equiv \langle IM|\hat{R}(\alpha,\beta,\gamma)|IK\rangle$ is an element of the Wigner D-matrix. This operator will restore good total angular momentum I and good magnetic quantum number M.

2.5.3 Restoration of angular momentum projection

To restrict the modelled nucleus to only rotate about one axis we need to replace the AMP operator (Equation (18)) to something more akin to the PNP operator (Equation (17)). This is because the group associated with global gauge rotations is the unitary group of degree 1. In the case of PNP the symmetry refers to a rotations in Fock space while in this case it refers to rotations (about one axis) in space. This Lie group is abelian and thus each irrep will have dimension $d^\mu = 1$ and has one parameter which we will call $\gamma \in [0, 2\pi]$ associating

it to the Euler angle γ describing the rotations about the z-axis. It follows that the volume is

$$v_G = \int_0^{2\pi} d\gamma = 2\pi.$$

The gauge rotations are represented by the unitary operator,

$$\hat{U}(\gamma) = e^{-i\gamma\hat{I}_z},$$

defined by the spin operator about the projected axis $\hat{I}_z$. It follows then that the projection operator for the irrep labeled by the desired quantum number M is,

$$\hat{\mathcal{P}}^M_z = \frac{1}{2\pi}\int_0^{2\pi} d\gamma\; e^{-i\gamma(\hat{I}_z - M)}. \tag{19}$$

This defines what we will call the restricted angular momentum projection (RAMP) operator, as it restricts the rotational symmetry of the system along one axis. To then implement this operator in a computational model we descretise it as:

$$\hat{\mathbb{P}}^M_{z,\,N_\gamma} = \frac{1}{N_\gamma}\sum_{n=1}^{N_\gamma} e^{-i2\pi\frac{n-\frac{1}{2}}{N_\gamma}(\hat{I}_z - M)}. \tag{20}$$

Here the we have introduced the number N_γ to define the partition size of the Riemann sum. Furthermore, the Riemann sum partition has been shifted by $\frac{1}{2}$ for better numerical stability and and to avoid any singularity at the origin.

The RAMP operator in the form of Equation (19) will extract the components of the state acted upon with M as eigenvalue of $\hat{I}_z$. However, the same can not be said in general for the discretised version (Equation (20)). With a large partition size, N_γ, it is possible that some components with eigenvalue different from the desired will be missed. It is found (cf. Appendix A) that $N_\gamma > \max(M - M_{\min},\ M_{\max} - M)$ is sufficient when $M_{\min}$ and $M_{\max}$ is the minimal and maximal spin components of the projected state respectively.

It is important to distinguish between γ as an Euler angle and γ as a collective variable. These symbols refer to completely different quantities and must not be confused. The Euler angle γ is a rotation parameter describing the orientation of the nucleus in space, whereas the collective variable γ characterizes the triaxial deformation of the intrinsic shape. In most cases the intended meaning is clear from context, but as a general rule, unless stated otherwise, γ in the following discussion should be understood to denote the collective deformation parameter.

3 Method

The code developed and extended for this thesis is written primarily in Fortran, which remains well suited for large-scale numerical calculations. Most of the data visualization and analysis, however, was carried out using Python and Gnuplot. The investigative procedure was as follows. First a reasonable set of HFB basis states was generated and the RAMP operator was applied to decompose them into components of well-defined spin-quantisation quantum number M. To verify the accuracy of this projection, the spin expectation value was recalculated and compared with the value obtained before projection. Then the nuclear energy spectra was studied by solving the Hill-Wheeler equation for the projected HFB basis states using the AMP and RAMP operator respectively. This enables a direct comparison between the two models and, in turn, with experimental data. The Hill-Wheeler coefficients yield the collective wavefunctions from which the existence of γ-vibrations can be assessed.

3.1 The model

The model, to which the RAMP operator was implemented, has been recently developed in Lund [12, 13]. It utilises HFB states as a many body basis and describes nuclear properties by the use of projected GCM. A detailed description of the model is beyond the scope of this thesis, although the relevant parts have been introduced in the background Section 2.

3.2 Restriction of the model

It should be noted that the implementation of the RAMP operator in the code employs a different basis than what is presented in the background. This is done such that the implementation may fit well with the preexisting model. The main motivation for this change is cranking: we want the projection axis to be aligned with the cranking axis, which is the x-axis, and thus a substitution $z \to x$ is required. The operator defined in Equation (19) then takes the form,

$$\hat{\mathcal{P}}^M_x = \frac{1}{2\pi}\int_0^{2\pi} d\beta\, e^{i\beta M}\hat{R}(-\frac{\pi}{2},\beta,\frac{\pi}{2}). \tag{21}$$

Here the rotation operator $\hat{R}(-\frac{\pi}{2},\beta,\frac{\pi}{2})$ is used to define the unitary operator $e^{-i\beta\hat{I}_x}$. Note that the gauge angle has been switched too, from the Euler angle γ to the Euler angle β, in accordance to the switch of axes. The optimised discretised RAMP operator is,

$$\hat{\mathbb{P}}^M_{x,\,N_\beta} = \frac{1}{N_\beta}\sum_{n=1}^{\frac{N_\beta}{2}}\left[e^{i2\pi\frac{n-\frac{1}{2}}{N_\beta}M}\hat{R}(-\frac{\pi}{2},\beta,\frac{\pi}{2}) + e^{-i2\pi\frac{n-\frac{1}{2}}{N_\beta}M}\hat{R}^\dagger(-\frac{\pi}{2},\beta,\frac{\pi}{2})\right]. \tag{22}$$

4 Results

The following section summarises calculations for ^{24}Mg and ^{32}S. The ^{24}Mg analysis is more extensive, comprising of both a feasibility study of the RAMP operator and the use of the RAMP operator in this model and also a study on the dynamic symmetry breaking of nuclei. The ^{32}S results provide additional support for the latter: the model's effectiveness in describing γ-vibrations using the RAMP operator. These two nuclei were chosen because their relatively small size keeps the computational load manageable, ensuring that both memory usage and runtime remain low enough for a standard workstation.

A collection of 404 HFB basis states was used for the ^{24}Mg calculations, sampled as shown in Figure 2. Generating these states required several hours and thus it constitutes the primary computational bottleneck of the program as the restricted projection and mixing steps requires only minutes. This behavior contrasts sharply with the full AMP implementation for complete rotational symmetry restoration: a smaller run of 121 points timed the projection and mixing at about a day each. For the ^{32}S calculations a smaller set of 297 HFB basis states were sampled as shown in Figure 3.

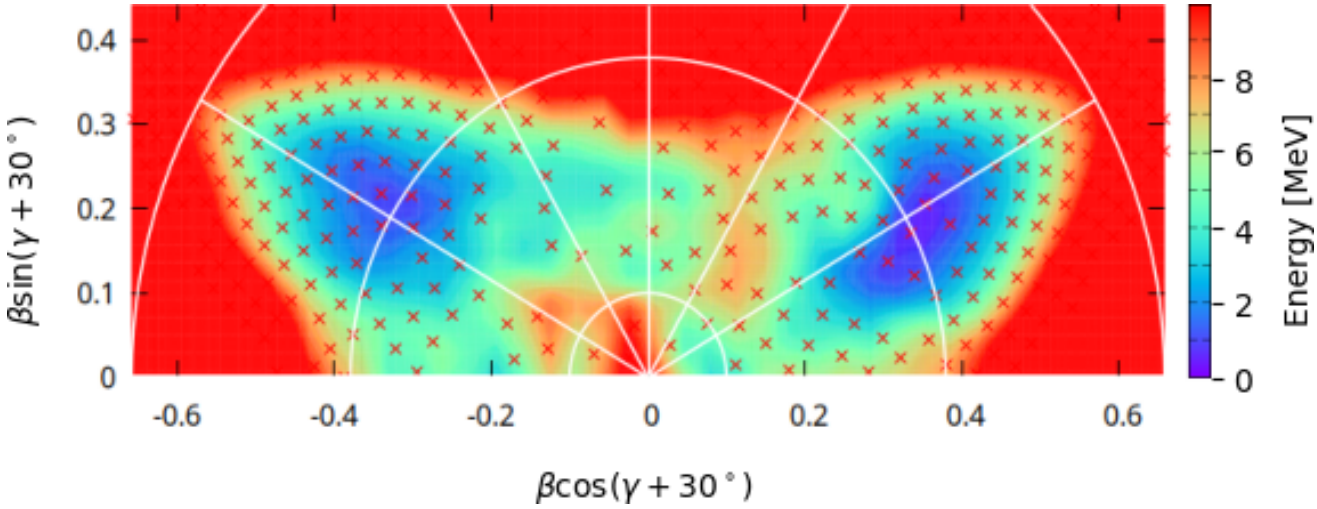

Figure 2: Energy surface for the sampling of the HFB basis states in the (β, γ)-plane, corresponding to ^{24}Mg. The red crosses indicate the different HFB basis states with energy shifted such that the minimum is set to 0 MeV. $\gamma = -30°$ is set along the positive x-axis and $\gamma = 60°$ the positive y-axis in accordance with the Lund convention[1].

The energy surfaces depicted in Figures 2 and 3 are defined by HFB basis states. These

[1]The Lund convention is a standard parameterization of nuclear quadrupole deformation using coordinates (β, γ), mapping the overall shape deformation magnitude via β and the degree of triaxiality via γ. Cartesian plotting coordinates are defined as $X = \beta\cos(\gamma + 30°)$ and $Y = \beta\sin(\gamma + 30°)$. This positions $\gamma = -30°$ (collective rotation around the short axis) along the positive x-axis and $\gamma = 60°$ (non-collective oblate rotation) along the positive y-axis.

states include additional variational parameters apart from β and γ, which explains the slight deviation from reflection symmetry in the $\gamma = 60°$ axis.

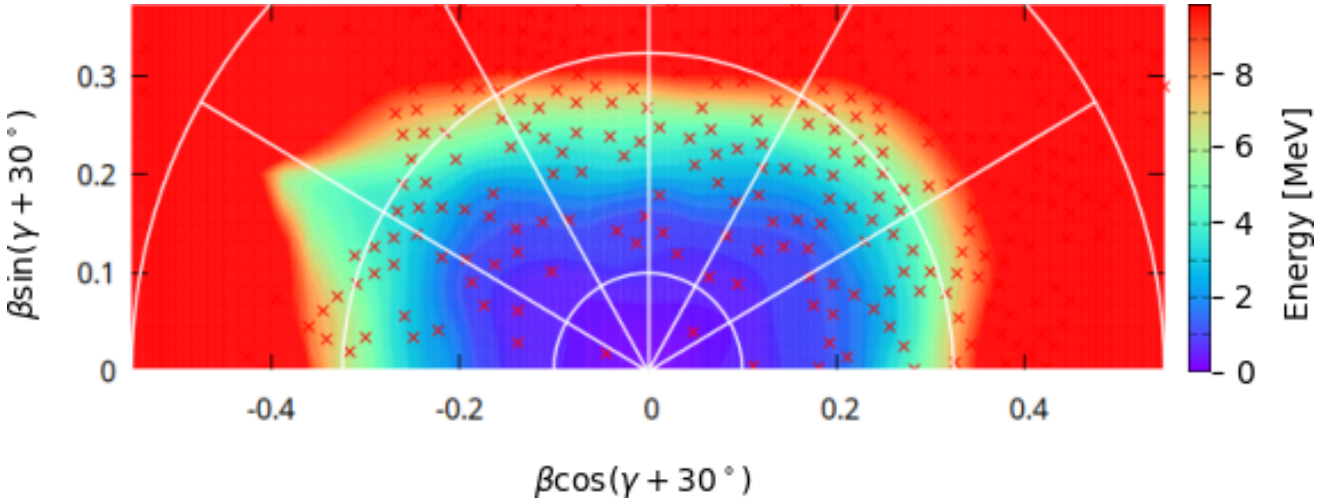

Figure 3: Energy surface for the sampling of the HFB basis states in the (β, γ)-plane, corresponding to ^{32}S. The red crosses indicate the different HFB basis states. $\gamma = -30°$ is set along the positive x-axis and $\gamma = 60°$ the positive y-axis in accordance with the Lund convention.

Before proceeding, it is important to clarify that the "collective wavefunctions" shown later on are not collective wavefunctions in the strict sense, since they are not amplitudes related to orthogonal states. They are heatmaps constructed from the solutions of the Hill–Wheeler equation. And these heatmaps visualize the square of the Hill-Wheeler coefficients, h_λ (see Equation (9)), associated with the collective coordinates used in the GCM. They therefore indicate the collective wavefunction in deformation space, but not the intrinsic many-body wavefunction of the nucleus. However, taking non-orthogonality into account usually gives similar results [14] and thus, for simplicity, and to avoid overcomplicating the discussion, we will nonetheless refer to them as collective wavefunctions.

4.1 RAMP accuracy

Because the spin expectation value for every HFB basis state is constrained through the cranking method (Section 2.4), we are able to evaluate the distribution of angular momenta for cranked states. The probability amplitude for a state $|\phi_\lambda\rangle$ to have spin M is given by the diagonal elements of the overlap matrix $O^M_{\lambda\lambda} = \langle\phi_\lambda|\hat{\mathbb{P}}^M_x|\phi_\lambda\rangle$. These amplitudes serve as weights in a weighted sum used to recompute the expectation value, $\langle\phi_\lambda|\hat{I}_x|\phi_\lambda\rangle$.

The results of this procedure, first applied without temperature excitation, are shown in Figure 4. For the vast majority of states, the two spin expectation values agree within $0.05\hbar$.

There are some outliers where all but two are bounded by $0.3\hbar$. These deviations do not necessarily indicate a flaw in the projection operator, $\hat{\mathbb{P}}^M_x$, as there is no clear correlation between the magnitude of the discrepancy and the spin value itself. However, a visible trend with respect to the HFB index suggests that this mismatch may stem from the reexpansion of the wavefunctions prior to projection. Furthermore, this trend can be explained by the fact that a higher HFB index correlates with a larger β deformation, which in turn leads to a more well-defined spin structure.

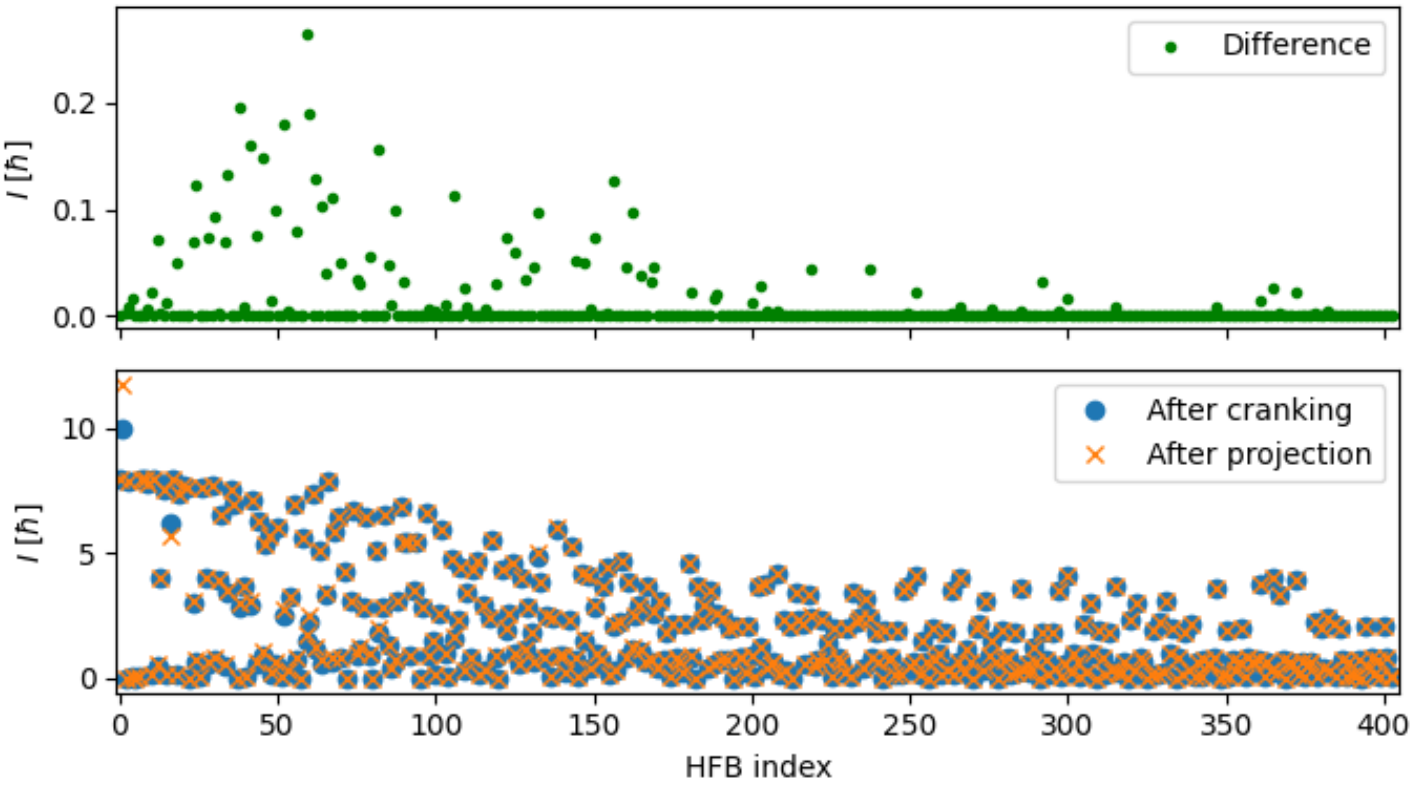

Figure 4: Spin expectation values for all sampled HFB basis states without temperature excitation. The blue dots show the spin of each state after cranking. Using the weights obtained from the projection method, a second spin expectation value is computed, indicated by the orange crosses. The green dots represent the difference between the two expectation values for each state neglecting the two outliers.

Temperature is introduced as a physically consistent and computationally feasible way to describe an excited nucleus within the HFB framework. This is done by way of including quasi-particle excitations and results in the capture of more spin states which is shown in Figure 5. This effect can be seen more clearly when decomposing the individual probability amplitudes for some specific state.

The HFB ground state, the HFB basis state found nearest the energy surface's rightmost

minima shown in Figure 2, has deformation parameters $\gamma \approx -2.9°$ and $\beta \approx 0.38$, with a cranked spin value of $M \approx 0.00772749\hbar$. Figure 6 shows this state decomposed into eigenstates of the spin projection operator, $\hat{I}_x$, using the probability amplitudes obtained from the RAMP operator. The resulting spin expectation value, $M \approx 0.00772743\hbar$, as calculated with the ascertained probability amplitudes, is in very good agreement with the expectation value of cranked state.

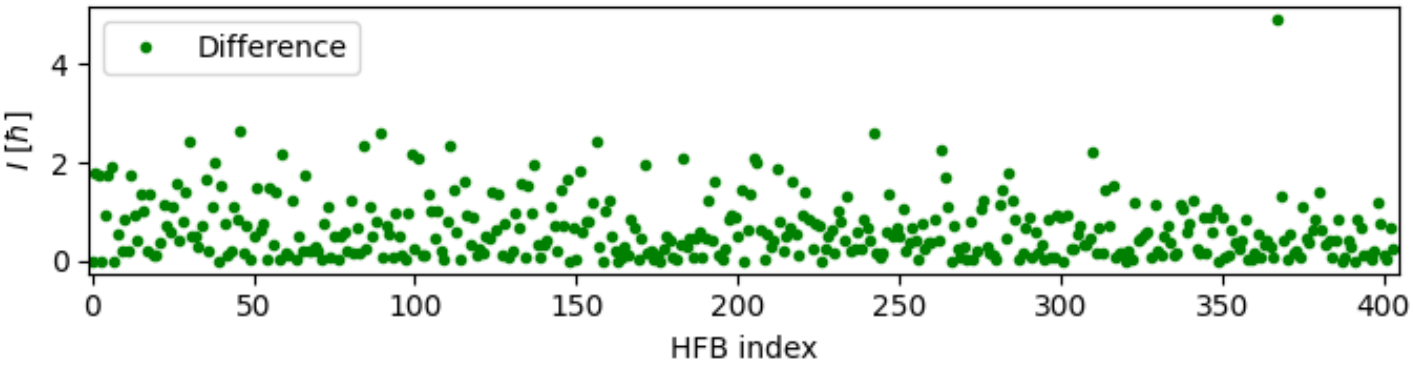

Figure 5: The system is first cranked to obtain an initial spin expectation value. After introducing temperature through quasi-particle excitations, the projection method yields the weight distribution for each quantum number M. Using these weights, a new spin expectation value is calculated. The green dots show the difference between the two expectation values for each HFB basis state.

When temperature is introduced, the spin decomposition broadens and shifts, as illustrated in Figure 7. This redistribution leads to a new expectation value of $M \approx 0.5$.

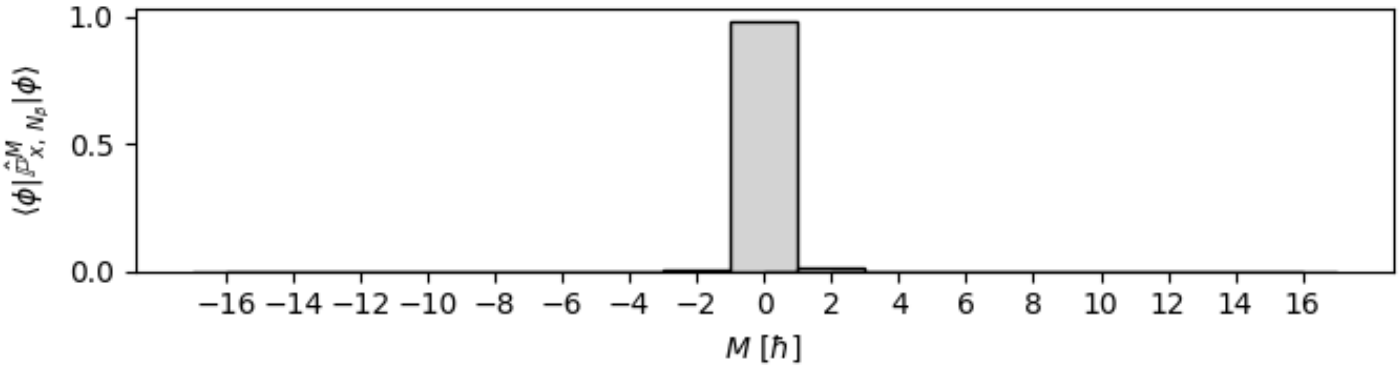

Figure 6: The probability amplitude for the HFB ground state to have spin M without temperature excitation.

The increased spreading also produces a non-negligible $M \neq 0$ components which in isolation

corresponds to a different energy than that of the original HFB state. Using, $E = \frac{\langle\phi|\hat{H}\hat{\mathcal{P}}^M_x|\phi\rangle}{\langle\phi|\hat{\mathcal{P}}^M_x|\phi\rangle}$, the energy of the HFB ground state projected onto $M = 0$ is found to be approximately 13.6 MeV higher than the unprojected value. This increase is also seen in the zero-temperature calculation, where the corresponding rise is about 4.0 MeV, despite the fact that the $M \neq 0$ components are almost entirely absent.

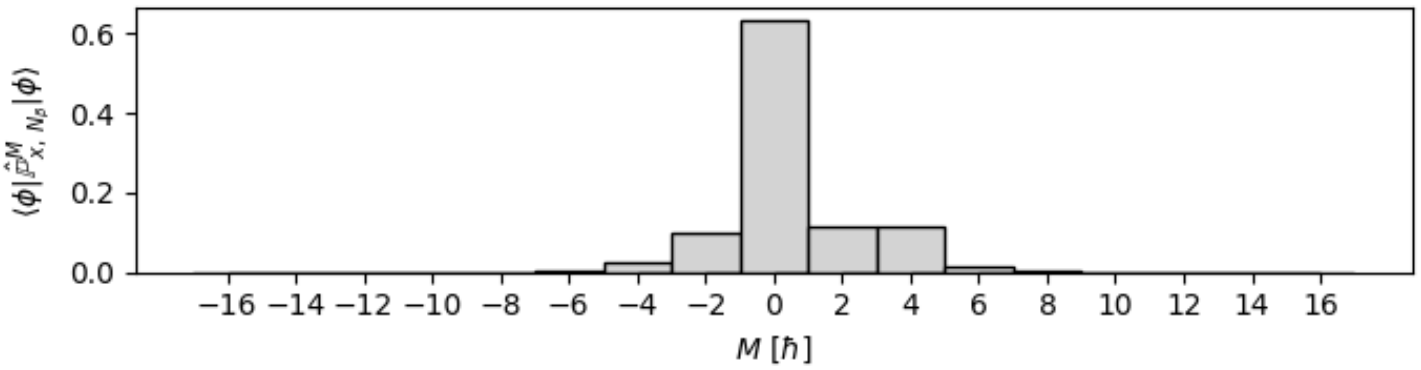

Figure 7: The probability amplitude for the HFB ground state to have spin M with temperature excitation.

4.2 Energy spectra

The Hill–Wheeler equation (Equation (9)) defines a generalised eigenvalue problem whose eigenvalues correspond to the calculated energy levels. These levels form the nuclear energy spectra shown in Figure 8. Two cases are considered: full rotational-symmetry restoration using AMP, and restricted rotational-symmetry restoration using RAMP. The AMP-derived spectra are referred to as the J-scheme, since the energies are plotted as functions of the total angular momentum J. In contrast, the RAMP-derived spectra are referred to as the M-scheme, because the energies are expressed in terms of the projected angular momentum M.

The observation made above, that the projected HFB ground-state energy is higher than the unprojected energy, is seen to hold for all basis states. This behaviour contrasts sharply with the J-scheme, where projection consistently lowers the energies due to the correlation energy gained from full rotational-symmetry restoration. This suggests that restricting the rotational symmetry to a single axis does not, by itself, improve the description of the system. However, the subsequent configuration mixing does recover correlation energy, although not to the same extent as in the J-scheme.

The M-scheme spectra also appear less satisfactory than the J-scheme, primarily due to the smaller number of energy levels obtained. This may indicate that additional statistics

(i.e. more HFB basis states) are required for convergence. Furthermore, when comparing the spin 0 spectra, the excitation energy of the first excited state, 0_1^+, is significantly larger in the J-scheme. If the 0_1^+ state in the M-scheme is excluded, however, the two spectra become much more consistent. We refer to such a state as a ghost, as it is best interpreted as an artefact originating in this case from the spin 2 yrast state, 2_1^+. This interpretation is supported by the analysis of the corresponding collective wavefunctions. By the same reasoning, the first excited spin 2 state, 2_2^+, is not considered a ghost, since its excitation energy agrees with the J-scheme and its collective wavefunction does not resemble that of the spin 6 yrast state 6_0^+.

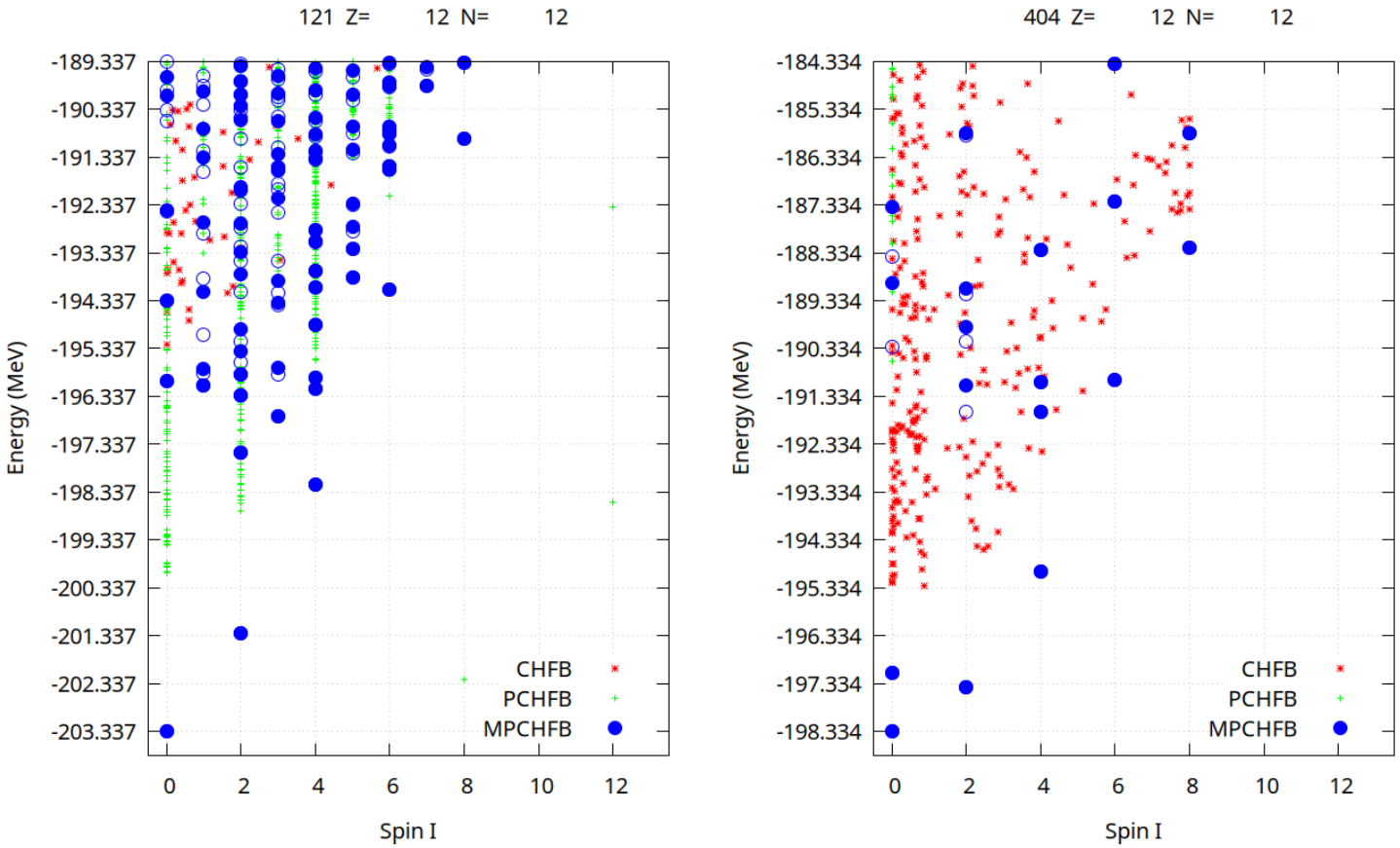

Figure 8: Calculated nuclear energy spectra for ^{24}Mg. To the left is the result in J-scheme, using the full AMP and 121 basis states. To the right is the result in M-scheme, using RAMP and 404 basis states. CHFB (red stars) are the constrained HFB basis states, PCHFB (green pluses) are the projections of the HFB states, and MPCHFB (blue dots) is the result of the mixing of the projected HFB basis states i.e. the Hill-Wheeler solutions.

We may compare these calculations with experimental data (taken from NuDat, Ref. [15]); for this purpose, the calculated spectra have been shifted such that the J-scheme ground state is set to 0 MeV. Figure 9 shows the calculated yrast line alongside the experimental

values. Notably, the restricted projection method provides more accurate results at higher spin. Although the model predicts yrast energies for spins above 8, these states do not follow the same systematic trend. This behaviour can be understood from Figure 4, which shows that almost all sampled HFB states have spin 8 or lower. Consequently, the predictive power at higher spin is strongly reduced. Even when temperature is introduced (Figure 5), only a small number of sampled states contribute significantly at high spin, thus limiting the reliability of the predictions in this region.

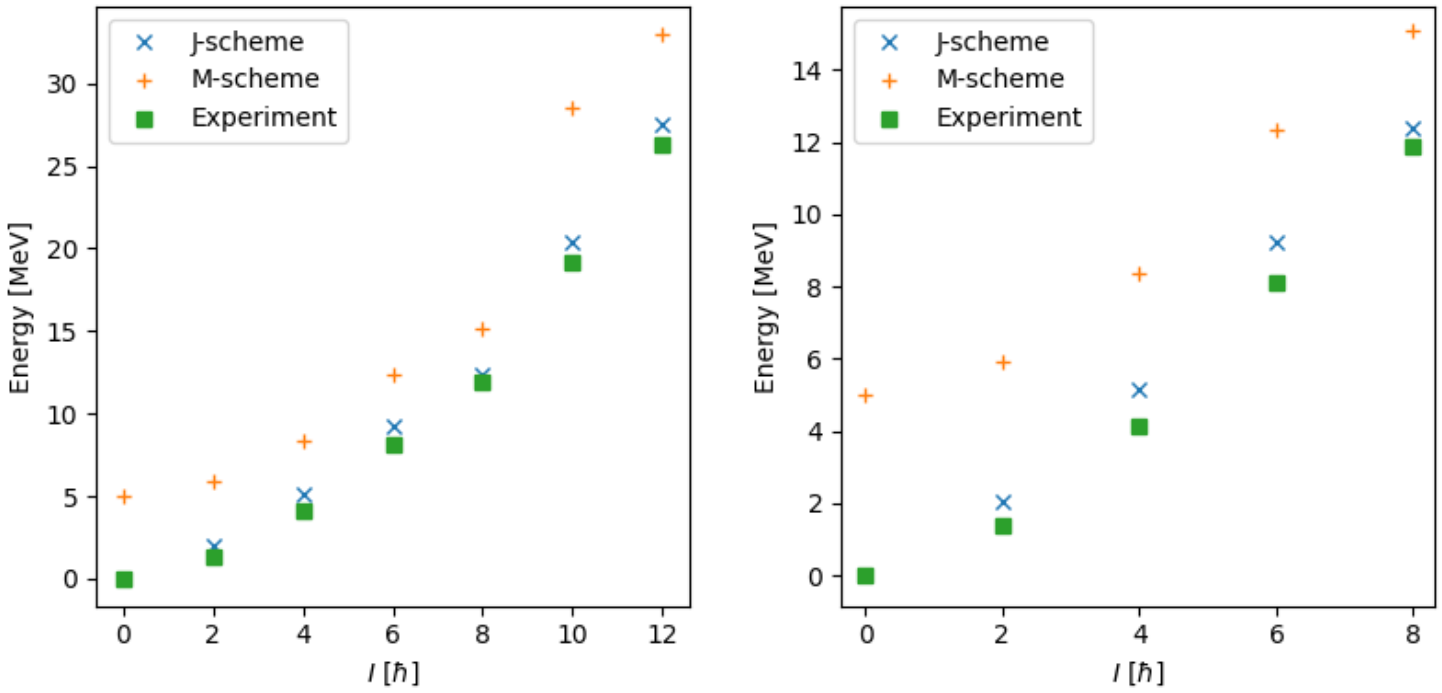

Figure 9: The yrast line as given by experimental data (green squares), calculated results from AMP restored spin (blue crosses) and calculated results from RAMP restored spin (orange pluses). Figure on the left is the full yrast line whilst the figure to the right depicts only spin 0 through 8.

4.3 γ-vibrations in ^{24}Mg

Considering the spin 2 yrast state, 2_1^+, and first excited state, 2_2^+, (the γ-band head), two collective wavefunctions are obtained from the J-scheme as shown in Figure 10. Their behaviour are as expected: the 2_1^+ state wavefunction exhibits a pronounced maximum about $\gamma = 0°$ whereas the 2_2^+ state displays two distinct maxima symmetrically separated about the $\gamma = 0°$ axis. When the projection is restricted to a single axis, the resulting collective wavefunctions persist, as shown by Figure 11. Although wavefunctions obtained by the M-scheme are more diffused than their J-scheme counterparts, they still reflect the same underlying structure,

consistent with a vibrational mode.

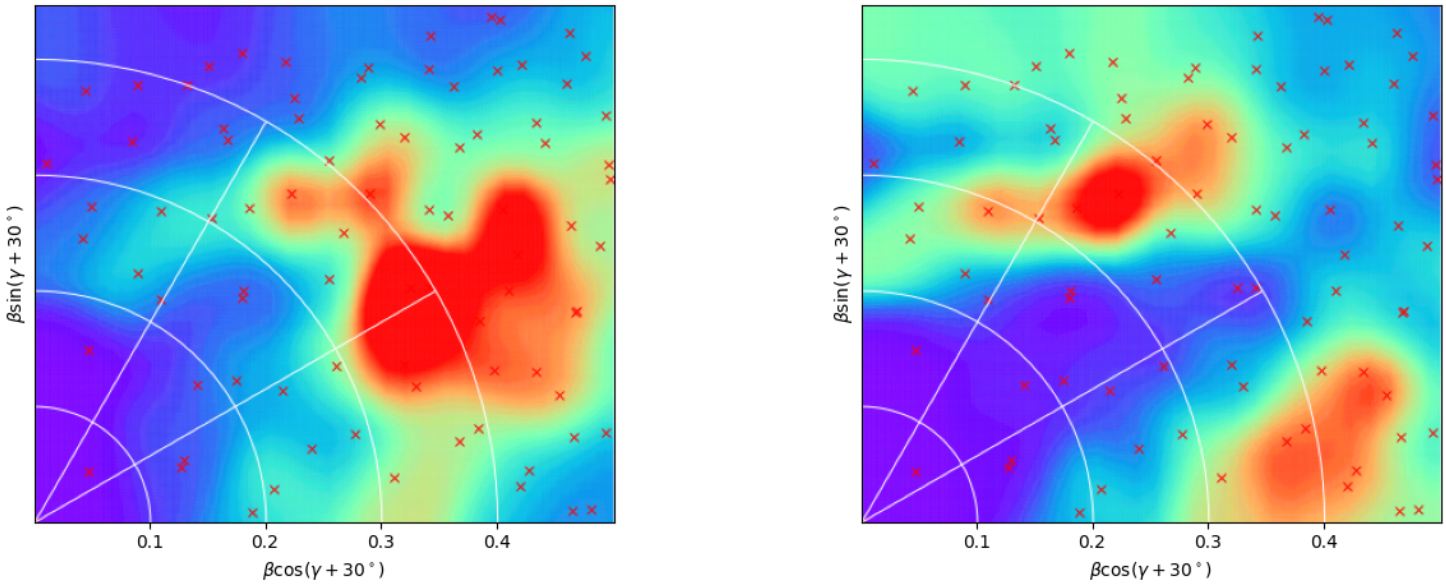

Figure 10: Collective wavefunctions for spin 2 as obtained by the full AMP. To the left is the 2_1^+ state and to the right is the 2_2^+ state. The red crosses indicate the sampled basis states. $\gamma = -30°$ is set along the positive x-axis and $\gamma = 60°$ the positive y-axis in accordance with the Lund convention.

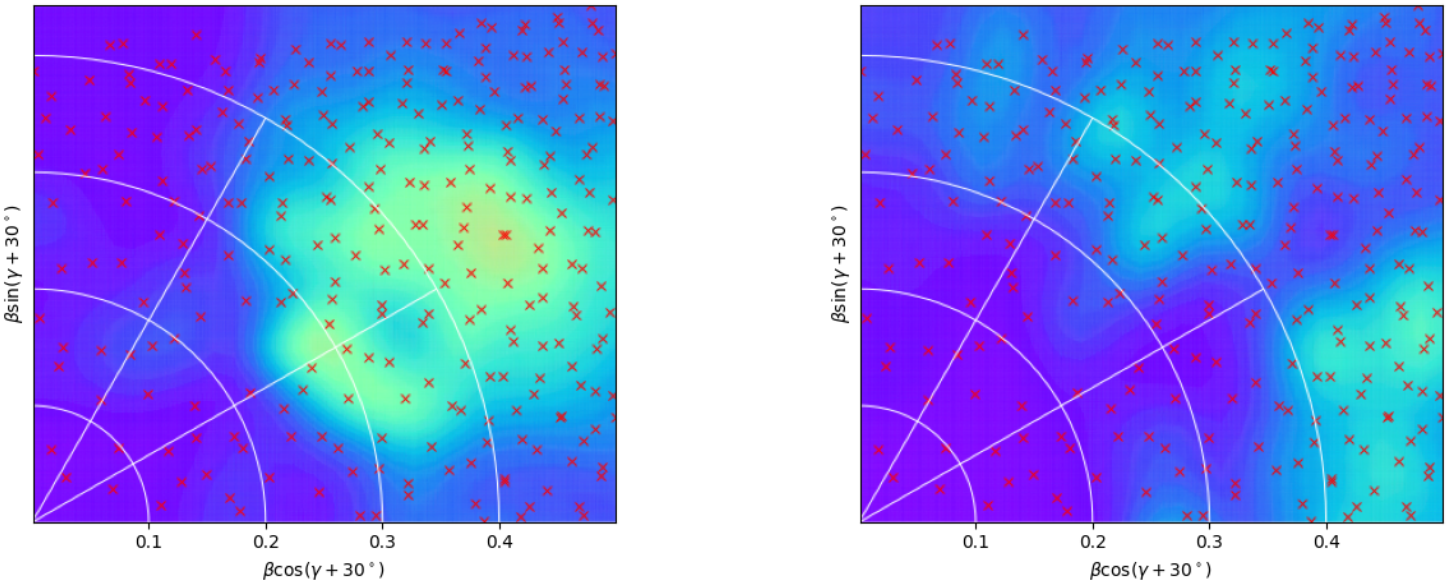

Figure 11: Collective wavefunctions for spin 2 as obtained by the RAMP. To the left is the 2_1^+ state and to the right is the 2_2^+ state. The red crosses indicate the sampled basis states. $\gamma = -30°$ is set along the positive x-axis and $\gamma = 60°$ the positive y-axis in accordance with the Lund convention.

To further clarify the results in Figure 11, the collective wavefunctions can be reduced to the γ degree of freedom by following a constant-β path through the maxima. Because the data is discrete, this path is implemented as a finite strip, segmented such that all basis states with γ values in the same interval contribute to a single binned point. Summing each element in the bin yields the corresponding γ-probability. The collective potential obtained from the HFB basis is treated analogously: only points within the same strip are considered, and the minimum in each segment defines the local potential well for the γ-vibrational motion. Using the energies obtained from the Hill–Wheeler equation (Figure 8), the resulting well and its vibrational modes can then be constructed, as shown in Figure 12.

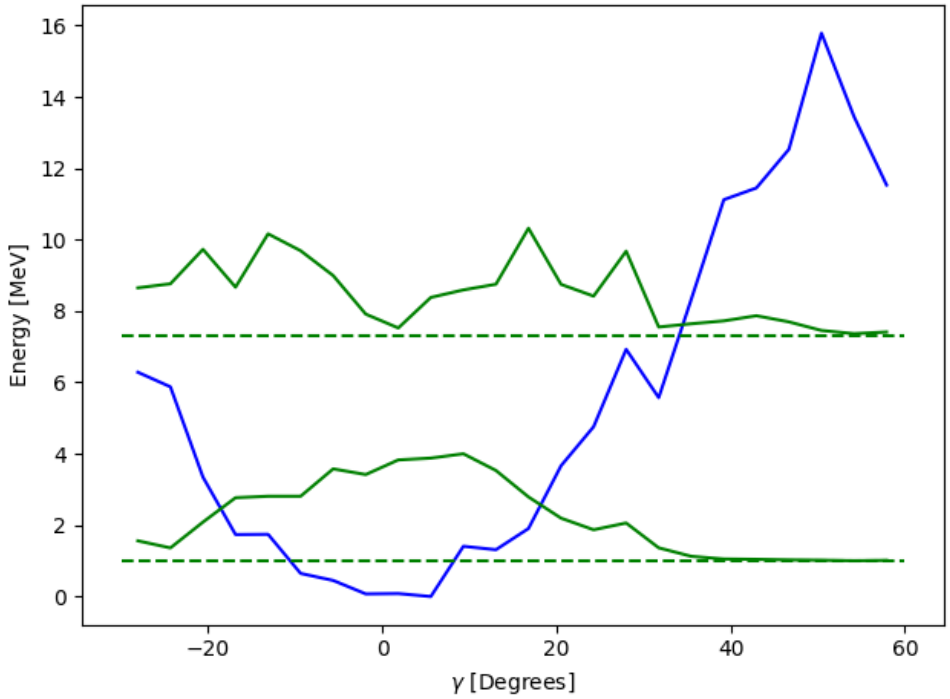

Figure 12: The potential well for ^{24}Mg is shown together with the two lowest vibrational modes, each plotted at its corresponding energy and shifted so that the 2_1^+ state lies at 1 MeV. The HFB potential (blue) and wavefunctions (green) are obtained from HFB basis states with $0.35 < \beta < 0.55$ and the γ degree of freedom is discretised into 24 bins each spanning 3.75°.

It should be noted that the γ-vibrational excitation energy ($E_\gamma = E_{2_2^+} - E_{2_1^+}$) used here is taken from the M-scheme which is calculated to be ≈ 6.32 MeV. This is done for consistency with the calculation for ^{32}S. However, as shown in Figure 8, this energy is slightly larger than obtained from the J-scheme, ≈ 3.79 MeV. This excitation energy is much closer to the experimental value of ≈ 2.87 MeV [15] and should be taken as the more correct value but for the analysis to come, consistency is preferred.

Furthermore, because the HFB basis states carry non-integer spin, ranging approximately from 0 to 8, it is more appropriate to construct the collective potentials using only the symmetry restored states. By evaluating,

$$\frac{\langle\phi|\hat{H}\hat{\mathcal{P}}^0_x|\phi\rangle}{\langle\phi|\hat{\mathcal{P}}^0_x|\phi\rangle} \quad \text{and} \quad \frac{\langle\phi|\hat{H}\hat{\mathcal{P}}^2_x|\phi\rangle}{\langle\phi|\hat{\mathcal{P}}^2_x|\phi\rangle}, \tag{23}$$

as the projected energies for each basis state, $|\phi\rangle$, one obtains revised collective potentials (these are shown in Figure 2). Ideally, the $M = 2$ projected potential should be used in Figure 12; however, the statistics within the relevant strip are too sparse for a reliable extraction. The HFB-derived potential nonetheless follows the same trend as the projected $M = 2$ potential, albeit appearing slightly softer. The loss of statistics with symmetry restoration is due to the effect of temperature excitations detailed in previous sections.

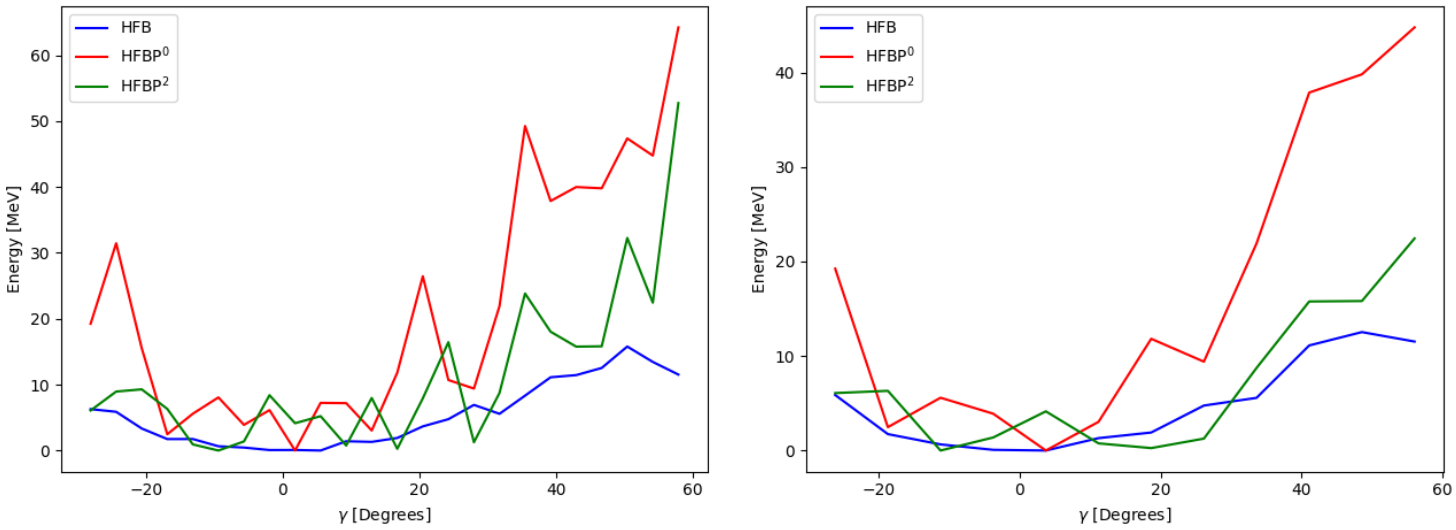

Figure 13: Comparison of the unprojected HFB potential (blue) with the spin projected potentials for $M = 0$ (red) and $M = 2$ (green) in ^{24}Mg. Both panels employ HFB basis states restricted to $0.35 < \beta < 0.55$. The left panel uses a 24-bin discretisation of the γ degree of freedom, whereas the right panel uses 12 bins.

4.4 γ-vibrations in ^{32}S

The calculation for ^{32}S was carried out without a corresponding J-scheme calculation, and the procedure followed is identical to that used for ^{24}Mg. The collective wavefunctions for the spin 2 yrast state, 2^+_1, and first excited state, 2^+_2, were obtained from the M-scheme, as shown in Figure 14. Their structure is characteristic of γ-vibrational modes: the 2^+_1 exhibits a pronounced maximum at $\gamma = 0°$, while the 2^+_2 state shows two distinct maxima

symmetrically displaced about the $\gamma = 0°$ axis.

Proceeding analogously to the analysis of ^{24}Mg we obtain the potential well for ^{32}S together with the two lowest γ-vibrational modes positioned at their respective energies. With the results for ^{24}Mg and ^{32}S now in hand, we may compare to the Bohr Hamiltonian using Equation (4). From the potentials shown in Figures 12 and 15 the stiffness ratio is estimated as $C_{22}^{Mg} \approx 2C_{22}^{S}$. That is, ^{24}Mg is about twice as stiff towards γ-deformations than ^{32}S. The increased softness in ^{32}S is expected to lower the γ-vibration energy, E_γ, which is observed when comparing Figures 12 and 15. Using these calculated Hill-Wheeler energies, $E_\gamma^{^{32}\mathrm{S}} \approx 3.49$ MeV and $E_\gamma^{^{24}\mathrm{Mg}} \approx 6.32$ MeV, we obtain the energy ratio ≈ 0.5525. And with the estimated stiffness relation, we obtain the expected ratio (4) to be ≈ 0.5564. The excellent agreement between these ratios further supports the interpretation of the calculated states as genuine vibrational excitations.

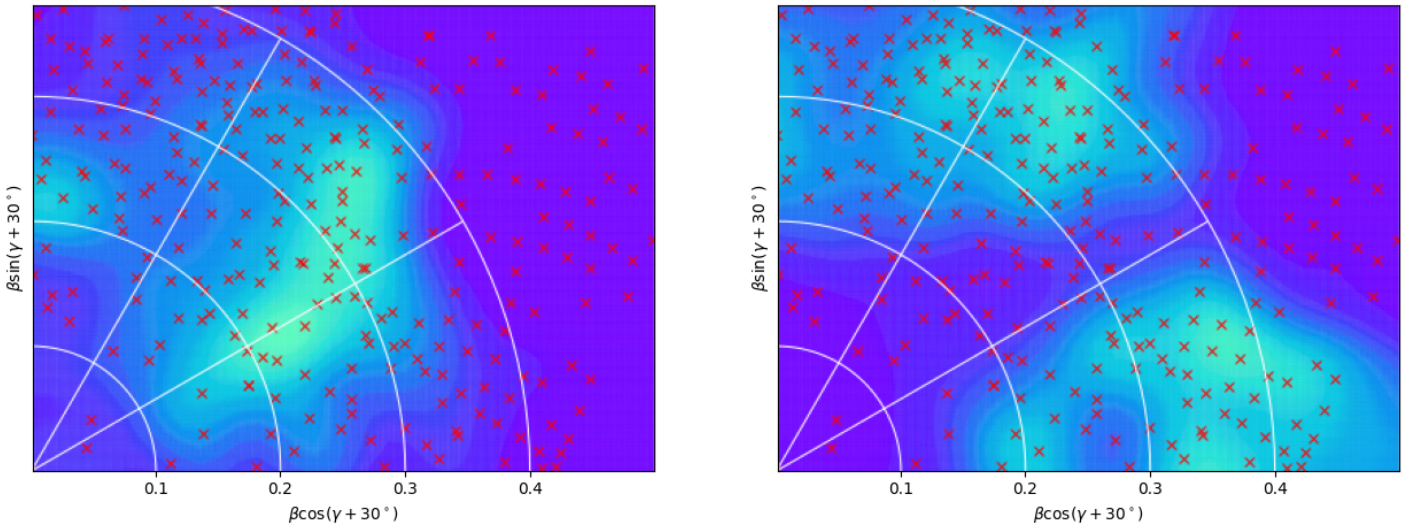

Figure 14: Collective wavefunctions for spin 2 as obtained by the RAMP. To the left is the 2_1^+ and to the right is the 2_2^+ state. The red crosses indicate the sampled basis states. $\gamma = -30°$ is set along the positive x-axis and $\gamma = 60°$ the positive y-axis in accordance with the Lund convention.

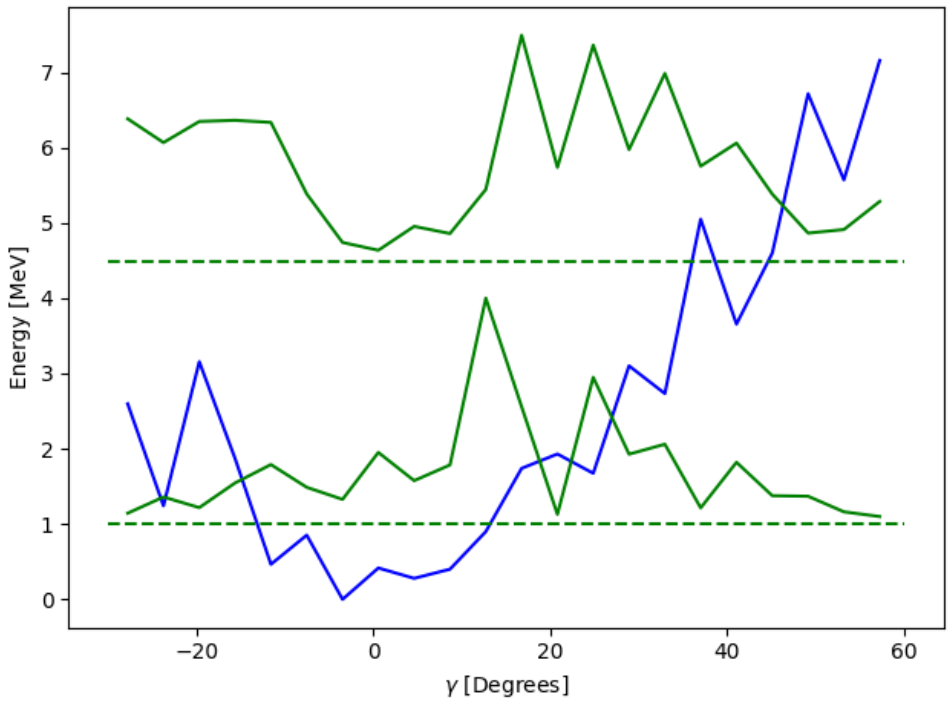

Figure 15: The potential well for ^{32}S is shown together with the two lowest vibrational modes, each plotted at its corresponding energy and shifted so that the 2_1^+ lies at 1 MeV. The HFB potential (blue) and wavefunctions (green) are obtained from HFB basis states with $0.3 < \beta < 0.5$ and the γ degree of freedom is discretised into 22 bins each spanning 4.1°.

5 Discussion

After applying the RAMP operator to the HFB basis states it is found that the spin expectation value, calculated using the probability amplitudes for each spin component, correspond very well to the cranked spin value. Although, there exists a nonzero set of HFB states that do not agree very well on this metric, in particular two states which differ by more then 0.3 $\hbar$. No apparent trend was observed relating this discrepancy with spin value; on the contrary, a trend relating the HFB index to both the number of, and magnitude in, the discrepancy was found. It is both the lack of the former trend and existence of the latter trend that lead to the conclusion that the issue does not lie with the implementation of the RAMP operator, nor the RAMP operator itself, but the more likely culprit is the reexpansion of the wavefunctions done before projection.

When comparing the two spectra, J-scheme and M-scheme, it is evident that the energies associated with the projected HFB basis states do not exhibit any gained correlation energy when the projection is performed using the RAMP operator, in contrast to the results obtained with the AMP operator. This behaviour was already apparent in the projected component of the HFB ground state: although the probability amplitude of the spin 0 component was almost completely 1, projection by RAMP still produced an unexpectedly high energy increase. One could make the argument that since a restricted projection about a single axis cannot recover the full rotational correlations the RAMP operator should not yield correlation energy in the same manner as the AMP operator. However, this reasoning does not completely explain the observations.

Moreover, it is plausible that the energy increases because the RAMP operator is a non-variational component extractor and removes alignment energy (minimised by the HFB method). The subsequent mixing of HFB basis states through the GCM does recover correlation energy, but only to a limited extent, compared to the J-scheme results. The resulting M-scheme spectra remain considerably less detailed than those of the J-scheme, despite being constructed from a much larger set of HFB basis states. A complete and satisfactory explanation to why this is was not found, however, it is expected that a larger HFB basis set would solve this issue.

This issue of correlation energy is also reflected in the comparison with the yrast line. A clear trend emerges in the M-scheme case: the yrast energy appears to converge as the spin increases. Since higher spin states have less correlation energy available to recover, the restricted projection is naturally expected to perform better in this regime.

It is also evident in the M-scheme spectra that the excited states cannot always be fully trusted, as higher spin configurations may be present low M components, producing degen-

erate states of any $M \leq J$. In some cases, such states can be identified by cross-referencing with another spectrum: any clear, isolated outlier is likely to be such an artefact. The method used here, comparing the collective wavefunctions of the suspected ghost state with those of the presumed physical state, is effective only insofar as the collective wavefunctions themselves are reliable and clearly different. A recurring theme throughout this work is that the M-scheme model requires substantially more statistics than the J-scheme. As a result, the collective wavefunctions obtained through the RAMP operator are far less pronounced than their AMP based counterparts, making this diagnostic method less dependable when used in isolation.

Most results, above the yrast line, cannot be regarded as fully reliable without contextual support from either a J-scheme calculation or experimental data. Nevertheless, with sufficiently large statistics, the M-scheme model could still provide a reasonable description of nuclear systems, benefitting from a significantly lower computational cost than the J-scheme approach. Moreover, its ability to describe higher-spin states without additional computational expense, combined with the accuracy trend observed at high spin, suggests that the M-scheme model retains potential value in specific applications.

When analysing the two lowest spin 2 states obtained from the M-scheme model, both nuclei ^{24}Mg and ^{32}S, exhibit behaviour characteristic of γ-vibrational modes. In the more comprehensive study of ^{24}Mg, the γ-vibration character observed in the J-scheme calculation persists in the M-scheme model, demonstrating that the observed double-maximum structure is not an artefact of rotational copies but reflects a genuine γ-vibrational excitation. Furthermore, the M-scheme calculation results agree closely with the Bohr Hamiltonian relation for the ratio of two γ-vibrational excitation energies.

Both methods are in principle exact for these states: the J-scheme allows for the definition of an approximate intrinsic frame composed of shapes rotated in all Euler angles to attain good total angular momentum, and the M-scheme allows to define an approximate intrinsic frame comprised of states with good angular momentum projection. M-scheme presents as a faster method due to the fact that the RAMP operator requires only one Euler angle as opposed to three in the case of the AMP operator hence the time difference is a linear scale as opposed to a cubic scale. Furthermore, the Hamiltonian and overlap matrices do not scale with spin in the M-scheme as opposed to the J-scheme thus also contributing to the speed difference. However, as detailed, there are some drawbacks that should be investigated further. As a diagnostic tool, to be used in tandem with the J-scheme, M-scheme serves as a cost effective method well suited for clearing up the ambiguity in characterising states as γ-vibrations.

6 Outlook

The principal objective of this thesis has been achieved: the question of whether γ-vibrations emerge naturally within a GCM-based framework can be answered in the affirmative. The methodology developed to address this question, namely, the M-scheme model constructed through the use of the RAMP operator, was tested and found to be well suited to the task, provided that the analysis is carried out with sufficient care and adequate statistical sampling. It should be noted, however, that this is not the only viable approach. For instance, one could investigate the time evolution of the γ-vibrational state to determine whether it exhibits genuine dynamical behaviour rather than representing a static deformation.

Several additional avenues for future work arise from the now-established M-scheme model. As discussed, if one seeks to obtain high-spin spectra with a reasonable computational cost, the M-scheme formulation may be advantageous, since the Hamiltonian and overlap matrices entering the Hill–Wheeler equation do not increase in dimension with spin in this framework. Moreover, if the projected potentials can be refined, it may become possible to strengthen the present conclusions by comparing the results with calculations based on the Bohr Hamiltonian using these projected potentials as a basis. A starting point would be to first examine the effect of the temperature excitations in correlation to the RAMP operator.

The scope of the present study has been limited, and an extension to a broader set of nuclei would further reinforce the conclusions drawn here. In addition, since the M-scheme intrinsic frame allows increased insight into the nature of γ-vibrational states, it would be of considerable interest to examine whether the $\gamma\gamma$-vibrations proposed to be observed experimentally in ^{164}Dy also emerge within this model.

References

[1] A. Bohr, *The coupling of nuclear surface oscillations to the motion of individual nucleons*. Munksgaard, 1952.

[2] A. Bohr and B. R. Mottelson, *Nuclear Structure Vol. II: Nuclear Deformations*. World Scientific, 1988.

[3] P. Ring and P. Schuck, *The Nuclear Many-Body Problems*. Springer, 1980.

[4] P. Möller, R. Bengtsson, B. G. Carlsson, P. Olivius, and T. Ichikawa, "Global calculations of ground-state axial shape asymmetry of nuclei," *Phys. Rev. Lett.*, vol. 97, p. 162 502, 16 2006. DOI: 10.1103/PhysRevLett.97.162502.

[5] T. Perissinotto et al., "Investigating two-non vibrational states in 162dy through coulomb excitation," *EPJ Web Conf.*, vol. 368, p. 00 006, 2026. DOI: 10.1051/epjconf/202636800006.

[6] J. Dobaczewski and W. Nazarewicz, "Hartree-fock-bogoliubov solution of the pairing hamiltonian in finite nuclei," *Fifty Years of Nuclear BCS (World Scientific, 2013) pp*, pp. 40–60, 2013.

[7] D. L. Hill and J. A. Wheeler, "Nuclear constitution and the interpretation of fission phenomena," *Phys. Rev.*, vol. 89, pp. 1102–1145, 5 1953. DOI: 10.1103/PhysRev.89.1102.

[8] D. R. Inglis, "Particle derivation of nuclear rotation properties associated with a surface wave," *Phys. Rev.*, vol. 96, pp. 1059–1065, 4 1954. DOI: 10.1103/PhysRev.96.1059.

[9] E. Noether, "Invariant variation problems," *Transport Theory and Statistical Physics*, vol. 1, no. 3, pp. 186–207, 1971. DOI: 10.1080/00411457108231446. eprint: https://doi.org/10.1080/00411457108231446.

[10] H. Hamermesh, *Group Theory and its applications to Physical problems*. Dover Publications, 1962.

[11] B. Bally and M. Bender, "Projection on particle number and angular momentum: Example of triaxial bogoliubov quasiparticle states," *Phys. Rev. C*, vol. 103, p. 024 315, 2 2021. DOI: 10.1103/PhysRevC.103.024315.

[12] J. Ljungberg, "Nuclear Structure from a Novel Beyond-Mean-Field Model : Towards Super-Heavy Nuclei from Densities and Mean-Fields to Wave Functions and Observables," eng, Ph.D. dissertation, Lund University, 2024, ISBN: 978-91-8104-135-4.

[13] J. Ljungberg, B. Carlsson, J. Rotureau, A. Idini, and I. Ragnarsson, "Nuclear spectra from low-energy interactions," *Physical Review C*, vol. 106, no. 1, p. 014 314, 2022.

[14] A. Idini, J. Ljungberg, J. Boström, and B. Carlsson, "Collective wavefunction of yrast states in 50cr," *IL NUOVO CIMENTO*, vol. 100, no. 31, p. 47, 2024.

[15] *National nuclear data center*, `http://www.nndc.bnl.gov/nudat/`, Accessed: 2026-04-20.

A Convergence of RAMP

We are tasked with checking the convergence of the descretised RAMP operator (20). Let us assume the state $|\Phi\rangle$ of broken angular momentum symmetry is a superposition of evenly weighted states $|M\rangle$ with good quantum number M (eigenvalues of the spin operator $\hat{I}_z$) which form an orthonormal basis. Since the norm of the state $|\Phi\rangle$ is not of interest we will omit the weights by setting them to 1, thus we have,

$$|\Phi\rangle = \sum_M |M\rangle. \tag{24}$$

Applying the discretised RAMP operator to eliminate all but the desired state $|M_0\rangle$, we can calculate the factor by which the weights of each state $|M\rangle$ are changed. The weight factor is,

$$w_{N_\gamma}^{I_{\text{tot}}M_0}(x) = \frac{1}{N_\gamma} \sum_{n=0}^{N_\gamma - 1} e^{-i2\pi \frac{n+\frac{1}{2}}{N_\gamma} x}, \tag{25}$$

where the difference in M-number has been introduced as x and the total angular momentum, I_{tot}, of the state $|\Phi\rangle$ is shown for clarity. A computational approach would be to plot these weights for each difference x and fixed total spin I_{tot} against the partition size N_γ. This method would visualise the convergence of the RAMP operator and has the advantage that it can be applied to the HFB basis states used in this thesis work. However, a more rigorous approach would be to derive the convergence analytically. The latter will be done in the following.

The weights, defined by Equation (25), is a geometric sum of the form,

$$s_N = \sum_{n=0}^{N} az^n. \tag{26}$$

We see if $z = 1$ then $s_N = (N+1)a$ and if $z \neq 1$ then $s_N(z-1) = a(z^{N+1} - 1)$. Thus, in our case, where $N = N_\gamma - 1$, $a = \frac{1}{N_\gamma} e^{-i\pi(M-M_0)/N_\gamma}$ and $z^{N+1} = e^{-i2\pi(M-M_0)} = 1$, we have,

$$\hat{\mathbb{P}}^{M_0}_{N,N_\gamma} = \frac{1}{N_\gamma} \sum_{n=1}^{N_\gamma} e^{-i2\pi \frac{n-\frac{1}{2}}{N_\gamma}(M-M_0)} = \begin{cases} 1 & M = M_0 + N_\gamma l \\ 0 & M \neq M_0 + N_\gamma l \end{cases} \tag{27}$$

Here l is an integer. From this we conclude that if we wish to restore all states with M-value between and including M_{min} and M_{max} then $N_\gamma > M_{max} - M_{min}$. However for each M_0 one needs only $N_\gamma > M_0 - M_{min}$ and $M_\gamma > M_{max} - M_0$.

B Reduction of integration domain of RAMP

The projection operator given in Equation (21) is

$$\hat{\mathcal{P}}_x^M = \frac{1}{2\pi}\int_0^{2\pi} d\beta\; e^{i\beta M} e^{-i\beta \hat{I}_x} \tag{28}$$

$$= \frac{1}{2\pi} e^{i\pi(M-\hat{I}_x)} \int_{-\pi}^{\pi} d\beta\; e^{i\beta M} e^{-i\beta \hat{I}_x} \tag{29}$$

$$= \frac{1}{2\pi} e^{i\pi(M-\hat{I}_x)} \int_0^{\pi} d\beta\; e^{i\beta M} e^{-i\beta \hat{I}_x} + \frac{1}{2\pi} e^{i\pi(M-\hat{I}_x)} \int_{-\pi}^{0} d\beta\; e^{i\beta M} e^{-i\beta \hat{I}_x} \tag{30}$$

$$= \frac{1}{2\pi} e^{i\pi(M-\hat{I}_x)} \int_0^{\pi} d\beta\; e^{i\beta M} e^{-i\beta \hat{I}_x} - \frac{1}{2\pi} e^{i\pi(M-\hat{I}_x)} \int_{\pi}^{0} d\beta\; e^{-i\beta M} e^{i\beta \hat{I}_x} \tag{31}$$

$$= \frac{1}{2\pi} e^{i\pi(M-\hat{I}_x)} \int_0^{\pi} d\beta\; e^{i\beta M} e^{-i\beta \hat{I}_x} + e^{-i\beta M} (e^{-i\beta \hat{I}_x})^{\dagger} \tag{32}$$

$$\tag{33}$$

And since we have enforced even signature we know that the prefactor $e^{i\pi(M-\hat{I}_x)} = 1$ and thus we obtain,

$$\hat{\mathcal{P}}_x^M = \frac{1}{2\pi}\int_0^{\pi} d\beta \left[e^{i\beta M} e^{-i\beta \hat{I}_x} + e^{-i\beta M} (e^{-i\beta \hat{I}_x})^{\dagger} \right] \tag{34}$$